View metadata, citation and similar papers at core.ac.uk
brought to you by CORE
provided by NOPR

Indian Journal of Geo Marine Sciences
Vol. 49 (02), February 2020, pp. 207-217

Prediction of shoreline changes in Almanarre beach using geospatial techniques

Minh Tuan Vu[1,2], Yves Lacroix[1,*], Van Van Than[3], & Viet Thanh Nguyen[4]

[1]SEATECH, University of Toulon, La Valette du Var, 83162, France
[2]National University of Civil Engineering, Hanoi, 100 000, Vietnam
[3]Thuyloi University, Hanoi, 100 000, Vietnam
[4]University of Transport and Communications, Hanoi, 100 000, Vietnam

*[E-mail: yves.lacroix@univ-tlf.fr]

Received 17 February 2017; revised 25 April 2017

In this study, the remote sensing and Geographic Information System (GIS) techniques coupled with the Digital Shoreline Analysis System (DSAS) is applied to detect the historical shoreline changes as well as to predict the future shoreline position along Almanarre beach which is being threatened by severe erosion. The results show that Almanarre beach suffered erosion with an average annual change rate of about -0.24 m/year over the period of 1973-2015. The most severe erosion was observed near Landmark B17 with the maximum erosion rate of -0.86 m/year. Moreover, the shoreline change in 2020 and 2050 are predicted at approximately -0.05 m/year and -0.22 m/year, respectively. The areas around Landmarks B06-08 and Landmarks B16-18 will be eroded with the maximum recession rates of -0.89 m/year and -0.94 m/year, respectively. This research proves that the combination of geospatial techniques and numerical model can be a reliable approach for investigating the shoreline change trend.

[Keywords: Accretion; DSAS; Erosion; Remote sensing; Shoreline extraction]

Introduction

The shoreline change is mostly controlled by natural causes or anthropogenic intervention, or both of them. The primary natural factors include waves, winds, currents, storm surge, sea level rise, and geomorphologic changes resulting from man-made factors through coastal construction, mining of beach sand, dredging of seabed sand, dam construction, or deforestation. The shoreline change results from coastal erosion or accretion which greatly affects human life along the coastal zone. Correspondingly, the detection and prediction of shoreline change is an essential task for protection of infrastructure and coastal zone management[1].

Until now, researchers have developed some approaches to investigate shoreline changes which can be divided into five categories. Firstly, historical map charts can reveal a historic information that is unavailable from other data sources, but many potential errors associated with these historical coastal records occur. Secondly, conventional field surveying can achieve high accuracy of measurement, but is labour intensive, time consuming and involves high cost[1]. Thirdly, aerial photographs can provide sufficient pictorial information. However, the frequency of data acquisition is not enough, temporal coverage is limited by depending on the flight path of the fixed-wing airplane; the photogrammetric procedure is costly and time consuming. Additionally, errors in shoreline interpretation may be introduced by the minimal spectral range of these sources[2]. At present, with rapid development of computational technology, the numerical models have become increasingly popular and have been successfully used to detect and predict the past and future shoreline evolution. They can be validated easily by measuring and observing the actual behaviour of the natural systems under the impacts of the wave climate, mean sea level, coastal defence works, etc. For instance, the project effects on the tidal current, tidal volume, sediment concentration and morphological evolution in Xiaomiaohong tidal channel, Jiangsu Coast, China were investigated by a two-dimensional numerical model and the result demonstrated that the change of morph-dynamic processes due to the reclamation project has only occurred near the project area and overall channel evolution was not significantly affected by this project[3]. Furthermore, Zheng et al.[4] developed a new model including interactions between waves and undertow and an empirical time-dependent turbulent eddy viscosity formulation that accounts for the phase dependency of turbulence on flow velocity and

acceleration. Gu et al.[5] introduced the Near CoM model coupling a Simulating Waves Nearshore model (SWAN), a nearshore circulation model (SHORECIRC), and a sediment transport model in a fully parallelized computational environment. The simulation results indicated that two factors contribute to the final double-sandbar morphology in different ways. Waves determine the final sandbar morphology, regardless of the antecedent bathymetry for energetic waves with high angles of wave incidence, whereas the pronounced morphological variability (crescentic pattern of sandbars) will control the evolution, which remarkably enhances the existing morphological patterns regardless of the changed wave condition for moderate waves with small angles of wave incidence. Nevertheless, using numerical models can be difficult for the establishment of boundary conditions, calibration coefficients and parameters regarding variables representing the reality of the system, that may generate the fail results[6]. In addition, the numerical modelling calculations are more time consuming than analytical and statistical calculations as well as the area of study domain are limited by the capacity of computer. Over the recent decades, remote sensing techniques are widely used and are more attractive as they have large ground coverage, are less time-consuming, inexpensive to implement, and also satisfactory acquisition repetition. Therefore, this technology becomes an effective solution for monitoring shoreline changes[7].

The shoreline of Almanarre beach lying on the western part of Giens tombolo, South France (Fig. 1(a)) has suffered both accretion and erosion processes caused by natural factors such as waves, winds and storm surge, or by human activities. By studying the submarine sediment logy, Blanc[8] showed that the waves caused the rapid degradation of the sandy spit in the western branch. Moreover, he uncovered the erosion at the sea bottom and the regression of Posidonia seagrass in the Giens gulf. Grissac[9] presented the research about dynamic sedimentology of Giens and Hyères bay. Through the *in situ* granulometric experiments as well as the analysis of wind and wave fields, he showed that there are two main longshore currents in the Gulf of Giens. The northern currents direct from west to east and from north to south, whilst the southern currents direct from south to north, then they follow the sandy spit to reach its centre. In addition, from the visual comparison of aerial photographs between 1955 and 1972, he also highlighted the significant decline of the western branch (down from 50 to 80 m in the center and 75-90 m in the south part) associated mainly with the degradation of Posidonia seagrass. Courtaud[10] used the aerial photographs and some field surveys to study the shoreline evolution of Giens tombolo. The study results showed that the zone from Landmark B01 to B23 (the northern part of Almanarre beach) was eroded with an average retreat of -6.4 m/ml corresponding to an erosion area of -13,900 m^2 during the period from 1950 to 1998, whilst the zone from Landmark B23 to B46 was accreted with an average advance of +19.8 m/ml corresponding to an accretion area of +41,100 m^2. In addition, Than[11] applied digital imagery processing techniques to find the average erosion annual rate of (-0.01 to -0.63) ± (0.27 to 1.82) m/year in the northern shoreline and the average accretion annual rate of (0.02 to 2.01) ± (0.14 to 5.1) m/year in the central and southern parts of the Almanarre beach over the period from 1920 to 2012.

In this research, the methodology of remote sensing and GIS technology along with DSAS was used to attain the main objectives: (1) quantify shoreline changes as well as accretion and erosion in Almanarre beach over the period from 1973 to 2015; (2) determine the main factor influencing the shoreline evolution of this area; and (3) predict the movement trends of shoreline in the future.

Materials and Methods

Study Area

The shoreline of Almanarre beach extends from north to south with the length of approximately 4.5 km through the Salt Road. According to the measurement data, the presence of deep cross-shore troughs and submerged shoals causes the complex bathymetry in the study area[10]. An average slope in the direction perpendicular to the shore is estimated from 1-1.5 % over the entire beach.

In the study area, the west and southwest winds play a decisive role in the coastal geomorphology and the wave agitation in Giens gulf. According to the wind data recorded at Hyères station (Fig. 1(a)), they blow with the total frequency of 25.66 % during the observation time. The winds coming from the west sector has the highest velocity 21.47 m/s with lower frequency, whereas the southwest winds maintain the highest frequency of 13.56 % with an average speed of 5.48 m/s. In addition to winds, waves have strong impact on the shoreline evolution of Almanarre beach. The west and southwest waves always attack the west

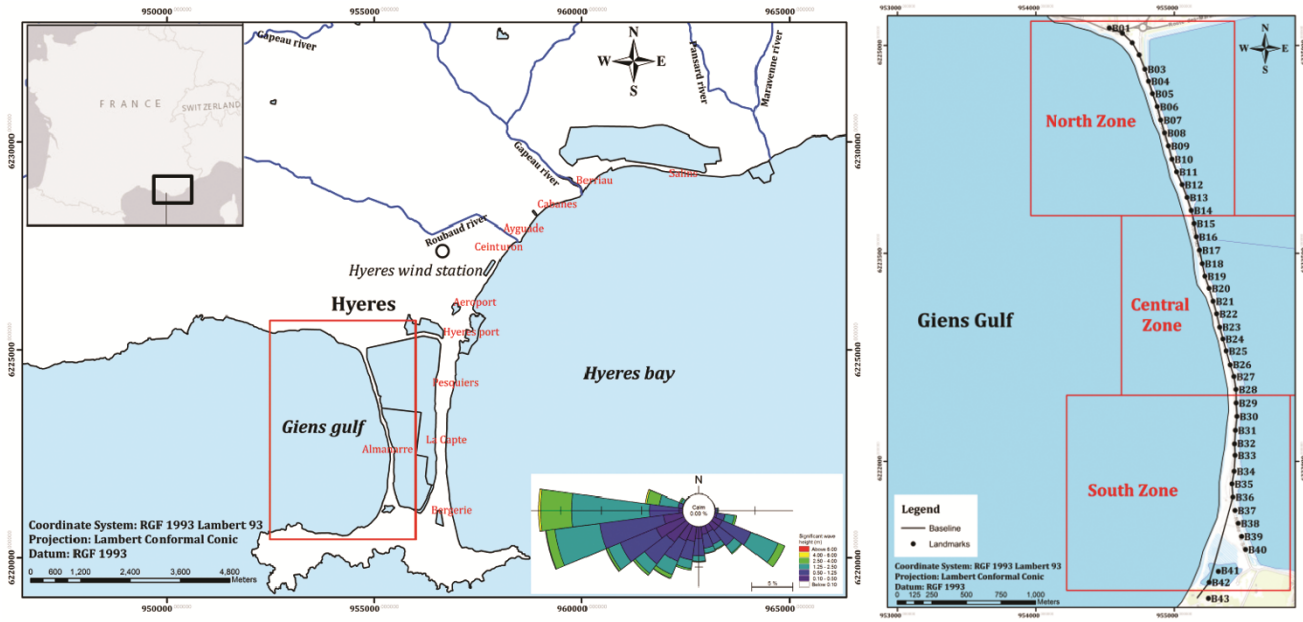

a. Location and annual swell rose b. The studied zones

Fig. 1 — The study area

coast of Giens tombolo with frequencies of 36.92 % and 28.84 %, respectively. The southwest waves generally have low energy with heights from 0.5 to 1.25 m and periods of less than 6 seconds occupying about 77 % of cases, whilst the waves coming from the west sector have medium energy with heights from 0.5 to 2.5 m occupying about 75 % of observed cases. Due to the largest tidal variation of less than 0.3 m, waves are the main factor acting on the hydrodynamic and sediment transport processes in the study area[12].

The oblique waves striking the coast of Giens tombolo generate the long shore current drift which redistributes sediment. The average current speed of long shore current varies from 3 to 7 cm/s in normal sea conditions and from 15 to 25 cm/s in stormy conditions at 4 m isobaths in the north zone of Almanarre beach. The dominant directions of long shore current on an average are from South to East and West to South, then they meet and mix together to generate cross-shore flow seaward at central zone of Almanarre beach[13]. Although some small streams flow in to the Giens Gulfs, between the points of Carqueiranne and Almanarre, the volume of sediment transported from them is not significant.

The principal sediment transport in the Giens Gulf starts from Almanarre in the north to Madrague of Giens in the south. Sediments are finer and finer with a decrease in the percentage of pebbles (from 55 % to 1 %) and well sorted (1.2 to 0.8 φ) southbound. However, the sector between Landmark B08 and B23 has a coarse grain size of 0.6 mm to 0.8 mm and a quasi-permanent and homogeneous sorting index due to the beach nourishment[10].

From the different characteristics of the geomorphology and the limitations of landmarks, the study area is separated by three main zones, namely, North zone, Central zone, and South zone (Fig. 1 (b)). The North zone of 1.5 km length is located between Landmark B01 and Landmark B14. The Central zone, 1.35 km long, starts from Landmark B15 up to Landmark B28 whereas the South zone with the length of 1.525 km spreads from Landmark B29 to Landmark B42.

Data Source

A series of satellite images such as Landsat 1 MSS, Landsat 4 TM, Landsat 7 ETM, and Landsat 8 OLI were acquired at non-equidistant intervals between 1973 and 2015. All the images have been collected almost at the same time in summer with good quality in order to exclude the effects of storm surge and waves. The details with respect to satellite images are listed in Table 1. However, the raw satellite images must be pre-processed by image enhancement (radiometric calibration, atmospheric correction, gap filling, pan-sharpening) and geometric rectification steps before being used as map base; because many defects, like radiometric distortion, wedge-shaped

Table 1 — List of satellite images used in the study

SI no.	Satellite and sensor	Acquisition date (dd/mm/yyyy)	Local time	Spatial Resolution (m)
1	Landsat 1 MSS	01/03/1973	09:51	79
2	Landsat 4 TM	27/08/1988	09:47	30
3	Landsat 7 ETM	28/08/2000	10:08	15/30
4	Landsat 7 ETM	18/08/2008	10:06	15/30
5	Landsat 8 OLI	30/08/2015	10:17	15/30

gaps, geometric distortion, presence of noise, etc., due to variations in the altitude, attitude, and velocity of the sensor platform usually occur in these images[14].

Analysis Methods

In order to extract shoreline from satellite images, several methods have been generated and developed. Firstly, a single band method can be used to map and extract shoreline from optical imagery. This method has some advantages, viz. the reflectance of water is almost equal to zero in reflective infrared bands, and the reflectance of absolute majority of land covers is greater than the water's[2]. However, the main disadvantage of this method is how to define the appropriate threshold value. Alesheikh et al.[2] proposed a new procedure for shoreline detection using a combination of band ratio and histogram thresholding techniques. Nonetheless, the shoreline moves toward water in some of the coastal zones and the procedure of extracting shoreline is quite time consuming. Another approach of extraction is by automation of shoreline detection which can be easily to apply and execute[15]. The main purpose of edge detection is to reduce the quantity of data and remove the irrelevant information in an image, but retain its structural properties. In this research, the shoreline position was mapped and extracted by using a nonlinear edge-enhancement technique with the Canny edge detector. The Canny edge detection is the most common edge detection method that performs well optimizing detection localization and number of responses criteria[16]. Due to the edge of the image corresponding to the discontinuity of the image grey value, the Canny algorithm is used to determine the pixels in the land-water boundary if their grey values have relatively large changes[17]. This technique gives an outstanding delimitation of the land-water boundary, and is time saving. The best colour composites of RGB (Red Green Blue) 567 (for Landsat MSS images), 543 (for Landsat TM and ETM+ images), and 652 (for Landsat OLI images) were be utilized for extracting the shorelines. These colour composites are improved to distinguish the objects clearly, such as between soil, vegetated land, and water, and hence they are easily digitized. The extracted shorelines were imported in DSAS module running in ArcGIS environment.

Although many methods were available in the DSAS, the most commonly used, LRR (Linear Regression Rate-of-change) statistic and EPR (End Point Rate) calculations, were hired to quantify the shoreline changes in Almanarre beach. Specifically, EPR was utilized for short term change analyses (1973-1988; 1988-2000; 2000-2008; 2008-2015), whereas LRR was applied for long term change analysis (1973-2015). Based on these settings, a total of 176 transects along the western tombolo were generated each 200 meters perpendicular to the baseline, at every 25 meters alongshore. Furthermore, intersection point coordinates between transect lines and shorelines as well as other statistical results were also computed by DSAS.

Finally, the distances between multiple historic shorelines and the baseline at each transect computed by DSAS was input into the code which the authors created to predict the positions of shorelines in 2020 and 2050. This code uses linear regression equation and runs in Matlab. The linear regression method which is used to define shoreline position change rate eliminates short-term variability and potential random error by using a statistical approach[18]. This method assumed that the observed periodical rate of change of shoreline position is the best determinant for prediction of the future shoreline. Its main shortcoming is that the sediment transport[19] and wave action are not taken into account because the cumulative impact of all the underlying processes is presumed to be captured in the position history[20]. To predict the future shoreline position, the baseline was first determined as the buffer of the shoreline in 2015. Next, transects casting perpendicular to the baseline at a user-specific spacing alongshore were generated by DSAS. Next, the intersection points between multi-temporal shorelines and transects were generated to input into the linear regression formula to determine the position of future shoreline at each transect. Finally, these positions were connected together to create the future shoreline[21].

$$y = a.x + b \quad \ldots (1)$$

Where:

y: Predicted distance from baseline,

x: The shoreline date,

a: Slope (the rate of change) and computed as follows:

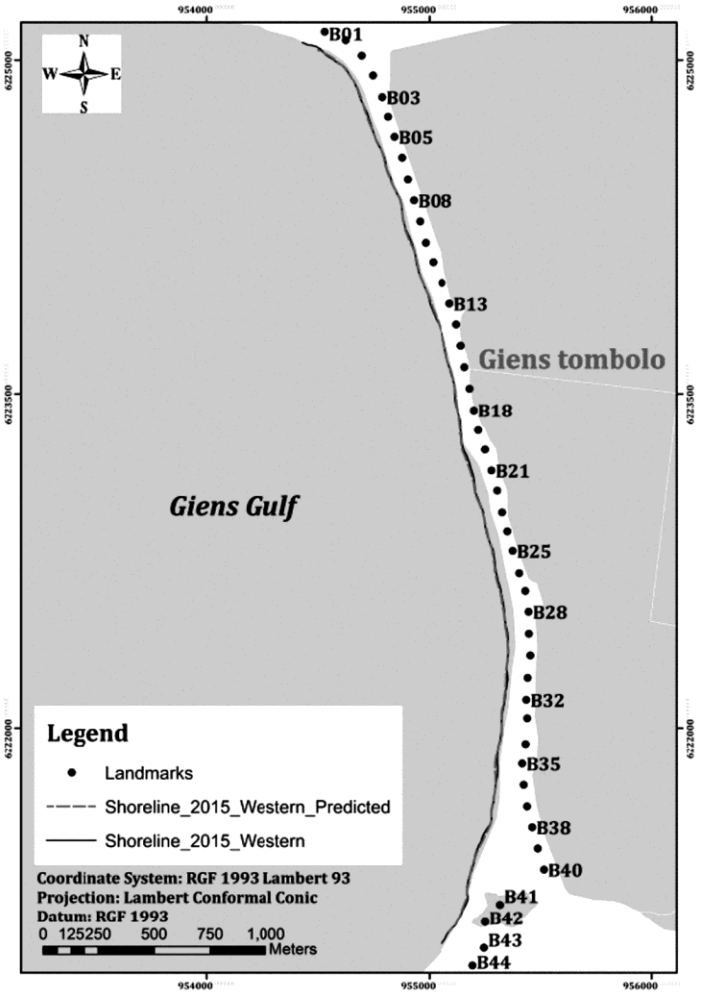

Fig. 2 — Actual shoreline position (2015) and predicted shoreline position (2015) along Almanarre beach with 5 m linear space transect.

$$a = \frac{n\sum_{i=1}^{n} x_i . y_i - \sum_{i=1}^{n} x_i \sum_{i=1}^{n} y_i}{n\sum_{i=1}^{n} x_i^2 - \left(\sum_{i=1}^{n} x_i\right)^2} \quad \ldots (2)$$

y_i: The distance from baseline to shoreline at date of x_i,
n: The number of shorelines,

b: y-intercept (where the line crosses the y-axis) and computed as follows:

$$b = \frac{1}{n}\left(\sum_{i=1}^{n} y_i - a.\sum_{i=1}^{n} x_i\right) \quad \ldots (3)$$

The accuracy and model quality were defined by using the cross-validation of the determined historical shoreline positions[22]. Particularly, the positional shift in the estimated shoreline of western Giens tombolo of 2015 was compared and validated with the extracted shoreline of 2015 from the satellite image. The results of validation are shown in Fig. 2. It is easily seen that the predicted shoreline is close to the actual one. The root mean square error (RMSE) for the entire shoreline of Almanarre beach was about 3.32 m. The value of this error is acceptable and reasonable; hence this method can be applied for predicting the position of future shorelines.

The accuracy of shoreline position as well as shoreline change rates can be influenced by several error sources. There are two kinds of uncertainties comprising positional uncertainty and measurement uncertainty. Positional uncertainties are related to the features and phenomenon that reduce the precision and accuracy of defining a shoreline position in a given year, viz. seasonal error E_s, and tidal fluctuation error E_{td}[23]. Seasonal error, E_s, is induced by the movements in shoreline position under the action of the waves and storms. Based on the measurement report of E.O.L[24], seasonal shoreline position differences between the spring and fall were estimated about ±5 m. The tidal

fluctuation error, E_{td}, comes from horizontal movement in shoreline position along a beach profile due to vertical tides. The base water level used to define the shoreline is the High Water Level (HWL). The study area is in a micro-tidal region with the tidal range less than 0.3 m, so this error can be neglected[25]. Regarding measurement uncertainties, they are associated with the skill and approach including digitizing error E_d, rectification error E_r and pixel error E_p[23]. Before digitization, the satellite images of 1973 and 1988 were re-sampled from 79 m to 15 m and from 30 m to 15 m, respectively without adding any spatial information. Hence, the digitizing errors were estimated about ±12 m for 1973, ±6 m for 1988 and ±3 m for remainders[26]. Finally, rectification error, E_r, is calculated from the orthorectification process.

According to Fletcher et al.[23], these errors are random and uncorrelated and can be represented by a single measure calculated by summing in quadrature. The total positional uncertainty, U_t, is:

$$U_t = \pm\sqrt{E_s^2 + E_{td}^2 + E_d^2 + E_p^2 + E_r^2} \quad \ldots (4)$$

The annualized uncertainty of shoreline change rate at any given transect was calculated as follows[27]:

$$U_a = \pm\frac{\sqrt{U_{t1}^2 + U_{t2}^2 + U_{t3}^2 + U_{t4}^2 + U_{t5}^2}}{T} \quad \ldots (5)$$

where U_{t1}^2, U_{t2}^2,…, U_{t5}^2 are the total shoreline position error for the various year and T is the 42 years period of analysis.

The maximum annualized uncertainty evaluated for individual transects is about ±0.67 m/year (Table 2).

Table 2 — Calculation of errors for different shorelines.

	1973	1988	2000	2008	2015
Seasonal error (E_s)	5	5	5	5	5
Tidal fluctuation (E_{td})	0	0	0	0	0
Digitizing error (E_d)	12	6	3	3	3
Rectification error (E_r)	12	9.9	7.35	10.8	6.75
Pixel error (E_p)	0.5	0.5	0.5	0.5	0.5
Total error (U_t)	17.70	12.62	9.40	12.28	8.93
Annualized error (U_a)	0.67 m/year				

Results and Discussion

Historical Shoreline Changes over Period of 1973-2015

Based on the short-term analysis for North Zone, the rate of change was measured along 1.5 km, from Transect 01 to Transect 61 corresponding to Landmark B01-B14, and both erosion and accretion were observed, but erosion is dominant (Fig. 3 (a)). In the period of 1973-1988, most of transects was deposited with the maximum accretion rate of about 1.51 m/year observed near Landmark B06. However, from 1988 to 2000, all transects in this zone suffered a severe retreat with the highest erosion rate of -2.13 m/year. The main reason of this phenomenon came from the high frequency of storms. There were 79 heavy seas and storms observed from 1992 to 1999[10]. This comment is valid for the other zones. The retreat trend was maintained in the periods of 2000-2008 and 2008-2015 with the highest erosion rates of -1.77 m/year and -2.89 m/year, respectively (Table 3). On the other side, the long-term analysis of 1973-2015 demonstrates that 90.16 % of transects were subjected to erosion, whereas only 9.84 % of those were prograded (Fig. 4). The high accretion rates are concentrated around Landmark B01 and B03 because the main long shore sediment transport oriented West-East is blocked by cross-shore submerged ridge. Inversely, the high erosion rates are recorded near Landmark B06 and B08 because this area is directly exposed to the strong waves from the southwest, with frequency of 28.84 %.

The central zone is composed of 54 transects over a total distance of 1.35 km, from Transect 62-115 in proportion to Landmark B15-B28. The short-term analysis indicates that this zone has been undergoing both accretion and erosion, as shown in Fig. 3 (b). In the 1973-1988 period, only area from Landmark B16 to 18 was eroded with the highest rate of -0.7 m/year. The remainders were prograded with the maximum accretion rate of 1.75 m/year. As the first zone from 1988 to 2000, most of transects in Central Zone was retreated at the mean rate of -1.27 m/year. Nevertheless, in the period of 2000-2008, 100 % of transects advanced seaward with the maximum accretion rate of 1.7 m/year (Table 3). The sudden positive shoreline change came from the beach replenishment in this period. According to the report of CERAMA[28], Giens tombolo suffered 12 storms from December 1999 to December 2008 in which the strongest storm approached Almanarre beach on 24th, January 2007. These storms caused severe erosion and breaching the salt road, especially between Landmark B13 to B18. Hence, a total of 10,000 tons of aggregates and nearly 10,400 m^3 of sand were used to nourish this area[11,12]. However, the beach nourishment only maintained the balance of this beach in the short time. The negative trend reappeared in the period 2008-2015 with the mean rate of -0.76

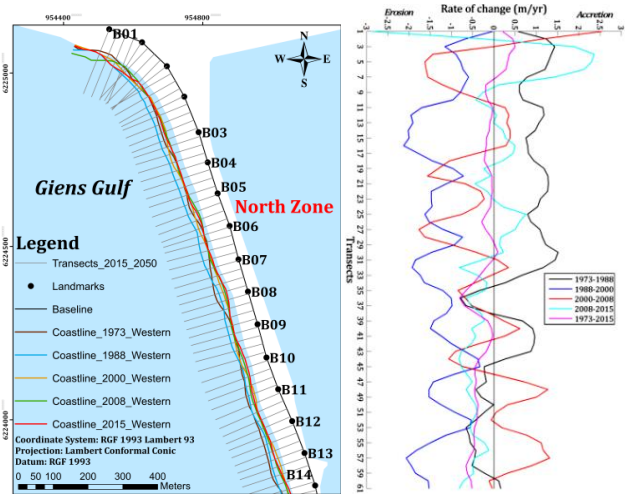

a. North Zone from Landmark B01-B14 (Transects 1-61)

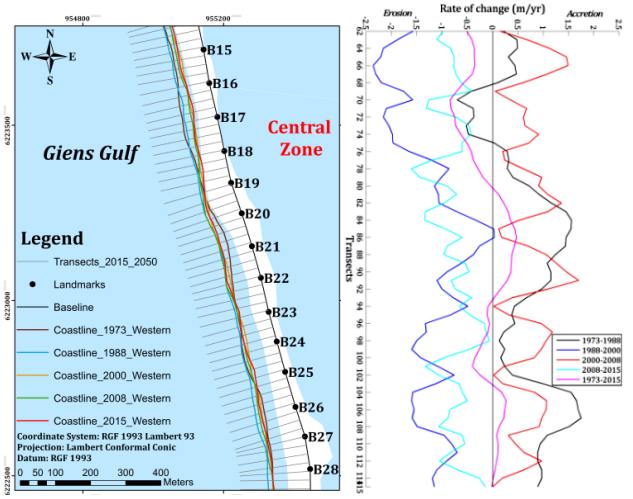

b. Central Zone from Landmark B15-B28 (Transects 62-115)

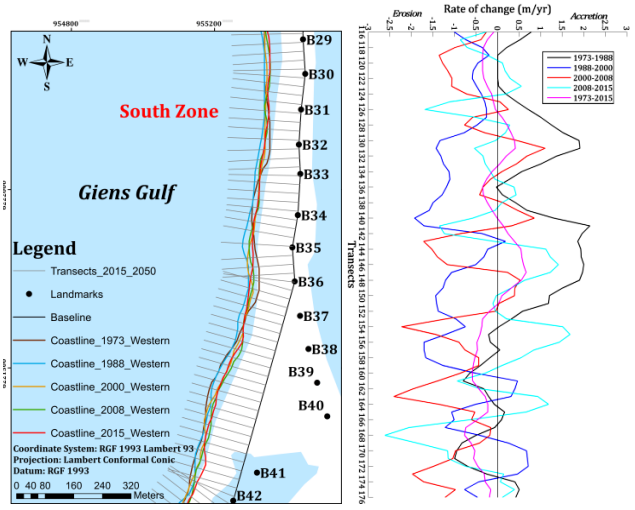

c. South Zone from Landmark B29-B42 (Transects 116-176)

Fig. 3 — Positions of shorelines and transect lines as well as shoreline change rates using EPR method along Almanarre beach over a period of 1973-2015

m/year. With regard to the overall shoreline changes, 61 % of transects record erosion and 39 % of transects record accretion. Erosion frequently occurred from Landmark B16 to B18 where deep trough nearly reaches the beach and the slope of the near shore zone is steeper. As a result, the waves approach the shoreline with high energy and take away sand from the beach. Moreover, this area is immediately influenced by the action combination of the southwest and west waves with total frequency of 65.76 %. Otherwise, the area from Landmark B19 to B29 is advancing with the highest accretion rate of 0.46 m per year induced by the cross-shore sediment transport channel[9].

The South Zone stretches over 61 transects (No. 116-176), corresponding to Landmark B29 to B42. Fig. 3 (c) represents the shoreline change of South Zone between 1973 and 2015. Generally, the erosion and accretion phenomenon happen alternatively, but erosion predominantly dominates in most of the transects. During the period of 1973-1988, the maximum erosion and accretion rates are -1 and 2.14 m per year, respectively. About 72 % of transects in this period were deposited with the mean rate of 0.51 m per year. Nonetheless, the long shore pattern was completely changed to erosion with mean rate of -0.74 m per year between 1988 and 2000. The negative trend was kept over the periods of 2000-2008 and 2008-2015 with the average erosion rates of -0.61 and -0.06 m/year, respectively (Table 3). Additionally, the long-term analysis reveals a slight accretion with the maximum rate of 0.46 m/year from Landmark B30 to B36 and erosion at the maximum rate of -0.71 m/year from Landmark B36 to B42 over the period of 1973-2015 (Fig. 4). According to Grissac[9], the cross-shore sediment transport in the Giens channel results in deposition in the area from Landmark B30 to B36. The eroded area may be provoked by the direct effect of northwest waves accompanied with the Mistral wind from the Rhone Valley.

The shoreline of Almanarre beach can be estimated in the short period of 2015-2020 and the long period of 2015-2050 by using linear regression analysis. In these periods, the shoreline change rates are predicted based on historical observations, but the special climate events, viz. sea level rise caused by global warming and tropical storms, have not been taken into account. Fig. 5 represents the positions of future shorelines and the shoreline change rates, whereas Table 4 summarizes statistical results of shoreline

Table 3 — The statistical summary of shoreline change rate for Almanarre beach over a period of 1973-2015

Zone	Period	Total no. of transects	Coast length (m)	Min rate (m/yr)	Max rate (m/yr)	Mean rate (m/yr)	No. of eroded transects	No. of accreted transects	% of eroded transects	% of accreted transects
	2015-2020	-1.77	2.59	-0.36	41	20	67.21	32.79	-1.77	2.59
North	2020-2050	-0.84	0.39	-0.32	55	6	90.16	9.84	-0.84	0.39
	2015-2050	-0.89	0.66	-0.33	58	3	95.1	4.9	-0.89	0.66
	2015-2020	-1.8	2.32	0.26	20	34	37	63	-1.8	2.32
Central	2020-2050	-0.87	0.46	-0.16	33	21	61.11	38.89	-0.87	0.46
	2015-2050	-0.94	0.67	-0.11	31	23	57.4	42.6	-0.94	0.67
	2015-2020	-2.5	2.62	0	29	32	47.54	52.46	-2.5	2.62
South	2020-2050	-0.72	0.47	-0.23	45	16	73.77	26.23	-0.72	0.47
	2015-2050	-0.91	0.54	-0.2	42	19	68.85	31.15	-0.91	0.54

Table 4 — Statistical summary of shoreline change rate for Almanarre beach over a period of 2015-2050

Zone	Period	Total no. of transects	Coast length(m)	Min. rate (m/yr)	Max. rate (m/yr)	Mean rate (m/yr)	No. of eroded transects	No. of accreted transects	% of eroded transects	% of accreted transects
	1973-1988			-0.79	1.51	0.53	19	42	30.65	69.35
	1988-2000			-2.13	-0.03	-1.27	61	0	100	0
North	2000-2008	61	1500	-1.77	2.55	-0.19	36	25	59	41
	2008-2015			-2.89	2.36	-0.1	42	19	68.85	31.15
	1973-2015			-0.83	0.38	-0.32	55	6	90.16	9.84
	1973-1988			-0.7	1.75	0.66	6	48	11.11	88.89
	1988-2000			-2.36	0.03	-1.27	52	2	96.3	3.7
Central	2000-2008	54	1350	0.02	1.7	0.74	0	54	0	100
	2008-2015			-1.61	-0.06	-0.76	54	0	100	0
	1973-2015			-0.86	0.46	-0.16	33	21	61.11	38.89
	1973-1988			-1	2.14	0.51	17	44	27.87	72.13
	1988-2000			-1.93	0.71	-0.74	52	9	85.25	14.75
South	2000-2008	61	1525	-2.41	1.1	-0.61	44	17	72.13	27.87
	2008-2015			-2.62	1.68	-0.06	31	30	50.82	49.18
	1973-2015			-0.71	0.46	-0.22	45	16	73.77	26.23

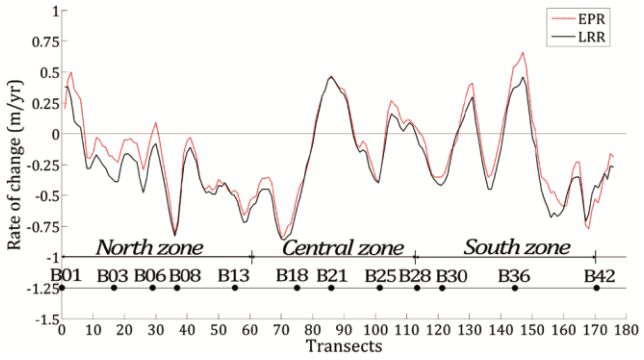

Fig. 4 — The variation of shoreline change rates using LRR and EPR methods along Almanarre beach over a period of 1973-2015.

Future Shoreline Changes over Period of 2015-2050

change assessment in Almanarre beach; they consist of the maximum, minimum and mean shoreline changes as well as % of accreted and eroded transects for periods: 2015-2020, 2020-2050, and 2015-2050.

Future Shoreline changes over period of 2015-2050

In the first region, North Zone, the shoreline recession is observed during all periods of 2015-2020, 2020-2050 and 2015-2050 (Fig. 5(a)) with the average erosion rate of -0.36 m/year, -0.32 m/year, and -0.33 m/year, respectively. All transects, except transect no 1-5 that are subjected to accretion, exhibit erosion in the period of 2015-2020 with the maximum retreat rate of -1.77 m/year around Landmarks B13 and B14. However, in the next periods of 2020-2050 and 2015-2050, the maximum recession rates are seen in the vicinity around Landmark B07-08 with the values of -0.84 m/year and -0.89 m/year (Table 4). This is the most vulnerable area to erosion in North Zone. Moreover, the % of eroded transects drastically increased over time, from 67.21 % in the period of 2015-2020 to 90.16 % in the period of 2020-2050.

In the next region, Central Zone, the results of statistical analysis obtained for 54 transects illustrate alternating areas of erosion and accretion, but majority of transects show erosion (Fig. 5(b)). During all the periods, the maximum erosion rates are mainly concentrated in the area between Landmarks B16 and

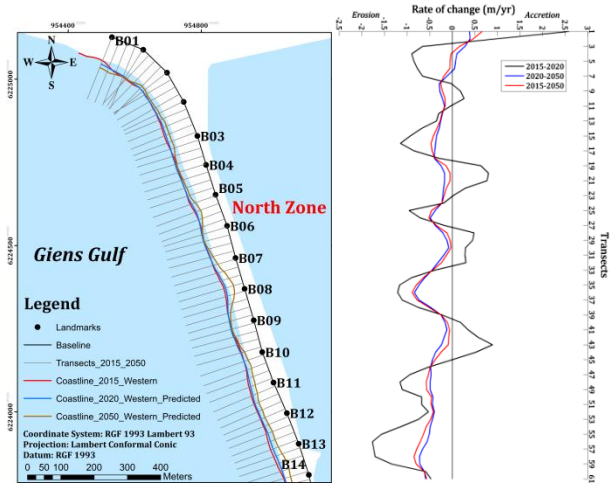

a. North Zone from Landmark B01-B14 (Transects 1-61)

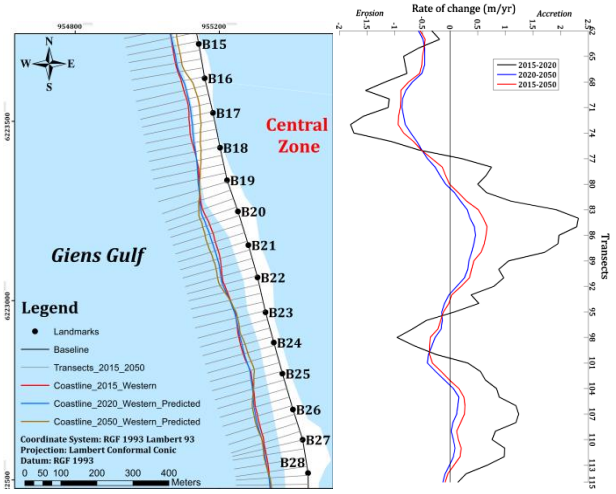

b. Central Zone from Landmark B15-B28 (Transects 62-115)

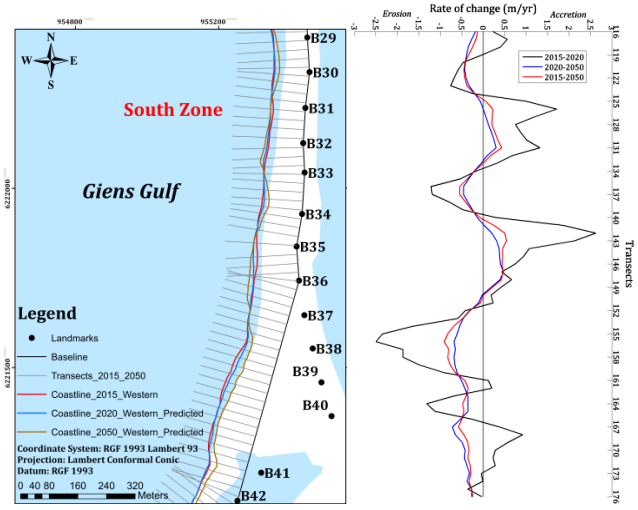

c. South Zone from Landmark B29-B42 (Transects 116-176)

Fig. 5 — Positions of shorelines and transect lines as well as shoreline change rates using EPR method along Almanarre beach over a period of 2015-2050.

B17, while the maximum progradation rates are observed between Landmarks B20 and B22 that coincide with the position of the cross-shore sediment transport channel. During 2015-2020, 62 % of the transects were accreted with the highest rate of 2.32 m per year at Landmark B20 and B22 that coincide with the position of the cross-shore sediment transport channel. During 2015-2020, 62 % of the transects were accreted with the highest rate of 2.32 m per year at Landmark B20 (Table 4). Nonetheless, the positive trend will be suddenly changed to the negative trend in the next periods. Particularly, 61.11 % of eroded transects are recorded with the highest rate of -0.87 m per year during the period 2020-2050, whereas the eroded transects are predicted at about 57.4 % with the highest erosion rate of -0.94 m per year between 2015 and 2050 (Table 4). Additionally, the prediction of future shoreline positions also revealed that the shoreline between Landmark B16 and B18 would be the most seriously eroded area.

For the South zone of Almanarre beach, a complex pattern of shoreline evolution is predicted with areas in erosion alternating with areas in accretion (Fig. 5(c)). During the period of 2015-2020, the eroded and accreted transects are almost the same with 48 % and 52 %, respectively. The maximum recession and accumulation rates are predicted about -2.5 m/year and 2.62 m/year (Table 4). The accretion areas are also forecasted in the vicinity of Landmarks B31-33 and B35-37. In the next periods of 2020-2050 and 2015-2050, erosion is dominant with the average rates of -0.23 m/year and -0.2 m/year, respectively. The maximum accretion rates are predicted to take place around Landmark B38-39, while the maximum erosion rates can be observed near Landmark B35-36. Finally, (Fig. 5 (c) also shows that the area between Landmark B37 and B42 could be subjected to severe erosion in future.

The study on the shoreline changes in Giens tombolo from 1973 to 2015 reveals that alternate accretion and erosion occurred along the shoreline of Almanarre beach, but erosion is dominant. Especially, most of transects along this zone were subjected to erosion from 2008 onwards. The main reasons of this recession are the action of waves on the near-shore bathymetry. Additionally, there is no sediment supply feeding the beach continuously, viz. no river mouths in the Giens gulf. The prediction of shoreline positions in 2020 and 2050 reveals that the erosive tendency will continue, particularly and severely in

the areas of Landmarks B07-08 and Landmarks B16-18. Finally, this study also demonstrates that the beach nourishment method only helps in the summer time and that too for the short term.

Conclusion

The study on the shoreline changes in Giens tombolo from 1973 to 2015 reveals that alternate accretion and erosion occurred along the shoreline of Almanarre beach, but erosion is dominant. Especially, most of transects along this zone were subjected to erosion from 2008 onwards. The main reasons of this recession are the action of waves on the near-shore bathymetry. Additionally, there is no sediment supply feeding the beach continuously, viz. no river mouths in the Giens gulf. The prediction of shoreline positions in 2020 and 2050 reveals that the erosive tendency will continue, particularly and severely in the areas of Landmarks B07-08 and Landmarks B16-18. Finally, this study also demonstrates that the beach nourishment method only helps in the summer time and that too for the short term.

Acknowledgment

This search was financially supported by the 911 Program of Vietnamese Ministry of Education and Training. The authors thank EOL, CETMEF, CEREMA, SHOM, and REFMAR for providing the bathymetric and hydrodynamic data. The USGS were appreciated for sharing the satellite images.

References

1 Tran, T.V. & Tran, T.B., Application of remote sensing for shoreline change detection in Cuu Long Estuary. *VNU J Earth Environ Sci*, 2009. 25.

2 Alesheikh, A., Ghorbanali, A., & Nouri, N., Coastline change detection using remote sensing. *Int J Environ Sci Technol*, 2007. 4(1): p. 61-66.

3 Zhang, C., Zheng, J., Dong, X., Cao, K., & Zhang, J., Morphodynamic response of Xiaomiaohong tidal channel to a coastal reclamation project in Jiangsu Coast, China. *J Coastal Res*, 2013. 65: p. 630-635.

4 Jinhai, Z., Chi, Z., Zeki, D., & Lihwa, L., Numerical Study of Sandbar Migration under Wave-Undertow Interaction. *J Waterw, Port, Coastal, and Ocean Eng*, 2014. 140(2): p. 146-159.

5 Gu, Z., Zhang, C., & Zheng, J., Influences of wave forcing and morphological variability on the evolution of a double-sandbar system. *Proc Inst Mech Eng, Part M*, 2015. 230(3): p. 467-480.

6 Pereira, C., Coelho, C., Ribeiro, A., Fortunato, A.B., Lopes, C.L., & Dias, J.M., Numerical modelling of shoreline evolution in the Aveiro coast, Portugal – climate change scenarios. *J Coastal Res*, 2013: p. 2161-2166.

7 Winarso, G., janto, J., & Budhiman, S., The potential application of remote sensing data for coastal study, in 22nd Asian Conference on Remote Sensing. 2001: Singapore.

8 Blanc, J.J., Recherches de sédimentologie littorale et sous-marine en Provence occidentale. 1958, *Université de Paris*: Masson et Cie. p. 140.

9 Grissac, A.J.D., Sédimentologie dynamique des rades d'Hyères et de Giens (Var). Problèmes d'Aménagements. 1975, *Université d'Aix-Marseille II*: Marseille. p. 86 + annexes.

10 Courtaud, J., Dynamiques geomorphologiques et risques littoraux cas du tombolo de giens (Var, France méridionale). 2000, *Université Aix-Marseille I*. p. 263.

11 Than, V.V., Modélisation d'érosion côtière : application à la partie Ouest du tombolo de Giens, in LATP. 2015, *Aix Marseille Université*: Marseille. p. 400.

12 SOGREAH, Etudes sédimentologiques de la rade d Hyères. Littoral de port Pothuau à la Badine. 1988. p. 68 + annexes et cartes.

13 Lacroix, Y., Than, V.V., Leandri, D., & Liardet, P., Analysis of a Coupled Hydro-Sedimentological Numerical Model for the Tombolo of GIENS. *Int J Environ Ecol Geol Geophys Eng*, 2015. 9(3): p. 117 - 124.

14 Lillesand, T.M., Kiefer, R.W., & Chipman, J.W., Remote sensing and image interpretation. 2008: *John Wiley & Sons*.

15 Loos, E.A. & Niemann, K.O. Shoreline feature extraction from remotely-sensed imagery. in *IEEE International Geoscience and Remote Sensing Symposium*. 2002.

16 Canny, J., A Computational Approach to Edge Detection. *IEEE Trans Pattern Anal Mach Intell*, 1986. PAMI-8(6): p. 679-698.

17 Liu, H. & Jezek, K.C., Automated extraction of coastline from satellite imagery by integrating Canny edge detection and locally adaptive thresholding methods. *Int J Remote Sens*, 2004. 25(5): p. 937-958.

18 Douglas, B.C. & Mark, C., Long-Term Shoreline Position Prediction and Error Propagation. *J Coastal Res*, 2000. 16(1): p. 145-152.

19 Michael, S.F., Dolan, R., & Elder, J.F., A New Method for Predicting Shoreline Positions from Historical Data. *J Coastal Res*, 1993. 9(1): p. 147-171.

20 Rongxing Li, J.-K.L.Y.F., Spatial Modeling and Analysis for Shoreline Change Detection and Coastal Erosion Monitoring. *Mar Geod*, 2001. 24(1): p. 1-12.

21 Nguyen, L.D., Minh, N.T., Thy, P.T.M., Phung, H.P., & Huan, H.V. Analysis of changes in the riverbanks of Mekong river-Vietnam by using multi-temporal remote sensing data. in *International Archives of the Photogrammetry, Remote Sensing and Spatial Information Science*. 2010. Kyoto, Japan.

22 Maiti, S. & Bhattacharya, A.K., Shoreline change analysis and its application to prediction: A remote sensing and statistics based approach. *Mar Geol*, 2009. 257(1–4): p. 11-23.

23 Fletcher, C.H., Romine, B.M., Genz, A.S., Barbee, M.M., Dyer, M., Anderson, T.R., Lim, S.C., Vitousek, S., Bochicchio, C., & Richmond, B.M., National assessment of shoreline change: Historical shoreline change in the Hawaiian Islands, in Open-File Report. 2012: Reston, VA. p. i-55.

24 E.O.L, Suivi de l évolution des plages de la commune Hyères-les-palmiers. 2000-2010: Commune de Heres-Les-Palmiers.

25 Rajasree, B.R., Deo, M.C., & Sheela Nair, L., Effect of climate change on shoreline shifts at a straight and continuous coast. *Estuar Coast Shelf Sci*, 2016. 183, Part A: p. 221-234.

26 Jayson-Quashigah, P.-N., Addo, K.A., & Kodzo, K.S., Medium resolution satellite imagery as a tool for monitoring shoreline change. Case study of the Eastern coast of Ghana. *J Coastal Res*, 2013: p. 511-516.

27 Hapke, C.J., Himmelstoss, E.A., Kratzmann, M.G., List, J.H., & Thieler, E.R., National Assessment of Shoreline Change: Historical Shoreline Change along the New England and Mid-Atlantic Coasts. 2011, *U.S. Geological Survey*. p. 57.

28 CERAMA, Details of the campaign 08301 and 08302-Porquerolles. 2014.